International Journal of Bifurcation and Chaos, Vol. 31, No. 8 (2021) 2150121 (20 pages)

DOI: 10.1142/S0218127421501212

Bifurcation Structures of Nested Mixed-Mode Oscillations

Munehisa Sekikawa
Department of Fundamental Engineering,
School of Engineering, Utsunomiya University,
Utsunomiya 321-8585, Japan
sekikawa@cc.utsunomiya-u.ac.jp

Naohiko Inaba
Graduate School, Electrical and Information Engineering,
Shonan Institute of Technology, Fujisawa 251-8511, Japan
naohiko@yomogi.jp

Received August 31, 2020; Revised December 2, 2020

In recently published work [Inaba & Kousaka, 2020a; Inaba & Tsubone, 2020b], we discovered significant mixed-mode oscillation (MMO) bifurcation structures in which MMOs are nested. Simple mixed-mode oscillation-incrementing bifurcations (MMOIBs) are known to generate $[A_0, B_0 \times n]$ oscillations for successive n between regions of A_0- and B_0-oscillations, where A_0 and B_0 are adjacent simple MMOs, e.g. $A_0 = 1^s$ and $B_0 = 1^{s+1}$, where s is an integer. MMOIBs are universal phenomena of evidently strong order and have been studied extensively in chemistry, physics, and engineering. Nested MMOIBs are phenomena that are more complex, but have an even stronger order, generating chaotic MMO windows that include sequences $[A_1, B_1 \times n]$ for successive n, where A_1 and B_1 are adjacent MMOIB-generated MMOs, i.e. $A_1 = [A_0, B_0 \times m]$ and $B_1 = [A_0, B_0 \times (m + 1)]$ for integer m. Herein, we investigate the bifurcation structures of nested MMOIB-generated MMOs exhibited by a classical forced Bonhoeffer–van der Pol oscillator. We use numerical methods to prepare two- and one-parameter bifurcation diagrams of the system with $m = 1, 2$, and 3 for successive n for the case $s = 2$. Our analysis suggests that nested MMOs could be widely observed and are clearly ordered phenomena. We then define the first return maps for nested MMOs, which elucidate the appearance of successively nested MMOIBs.

Keywords: Mixed-mode oscillation; mixed-mode oscillation-incrementing bifurcation; nested mixed-mode oscillation.

1. Introduction

Mixed-mode oscillations (MMOs) were first discovered in chemical experiments and have been studied extensively in recent years [Hudson *et al.*, 1979; Orban & Epstein, 1982; Maselko & Swinney, 1986; Albahadily *et al.*, 1989; Brøns *et al.*, 2008]. These oscillating systems periodically go through L large excursions followed by s small peaks; the notation "L^s" is used to distinguish oscillations. This definition of MMOs is ambiguous, but they appear universally in the extended slow–fast and multi-scale dynamics in which canard trajectories are seen [Brøns *et al.*, 2008; Petrov *et al.*, 1992; Yoshinaga *et al.*, 1988; Kuehn, 2015]. Canards were discovered in the early 1980s and represent a key discovery in nonlinear dynamics [Benoit *et al.*, 1981; Diener, 1984; Zvonkin & Shubin, 1984; Baer & Erneux, 1986, 1992; Braaksma & Grasman, 1993;

Arnol'd, 1994; Guckenheimer *et al.*, 2000]. Historically, MMOs have been discussed as a subset of canards. Numerical studies and experiments with circuits have established that canards appear in Bonhoeffer–van der Pol (BVP) oscillators [Itoh & Tomiyasu, 1990]. The dynamics of BVP oscillators are equivalent to those of FitzHugh–Nagumo systems [FitzHugh, 1961; Nagumo *et al.*, 1962]. However, Brøns *et al.* argued that MMOs were discovered experimentally more than 100 years ago, suggesting that the phenomena may appear more universally in slow–fast systems [Brøns *et al.*, 2008].

MMOs have been observed in various extended dynamics that can undergo a canard explosion, such as in noise-induced oscillatory dynamics near a relaxation oscillation [Ryashko, 2018; Sudhu & Kuehn, 2018; Muratov & Vanden-Eijnden, 2008], forced canards near supercritical [Kutafina, 2015] and subcritical Hopf bifurcation points [Shimizu *et al.*, 2011; Shimizu *et al.*, 2012; Shimizu *et al.*, 2015; Shimizu & Inaba, 2016a; Kousaka *et al.*, 2017; Inaba & Kousaka, 2020a; Inaba & Tsubone, 2020b], and extended three-variable canard-generating dynamics [Kawczyński *et al.*, 2000; Kawczyński & Strizhak, 2000; Petrov *et al.*, 1992; Rachwalska & Kawczyński, 2001; Sekikawa *et al.*, 2010; Shimizu & Inaba, 2016b; Yoshinaga *et al.*, 1988]. MMOs have been the subject of intense research in the last four decades [Scott, 1993; Brøns *et al.*, 2006; Krupa *et al.*, 2008; Markman & Bar-Eli, 1994; Brøns *et al.*, 1997; Sudhu & Kuehn, 2018; Muratov & Vanden-Eijnden, 2008; De Maesschalck *et al.*, 2014; Freire & Gallas, 2011a, 2011b; Desroches *et al.*, 2013; Guchenheimer & Scheper, 2011; Desroches *et al.*, 2012; Sekikawa *et al.*, 2010; Kousaka *et al.*, 2017; Takahashi *et al.*, 2018].

The mechanism behind simple MMOs have been elucidated in theory [Kuehn, 2015; Brøns *et al.*, 2006; Krupa *et al.*, 2008; Kutafina, 2015; De Maesschalck *et al.*, 2014; Guchenheimer & Scheper, 2011; Desroches *et al.*, 2012]. However, numerical studies of MMOs have revealed that extremely complex MMO bifurcations occur including strongly ordered phenomena that add MMOs to a system's trajectory. Kawczyński *et al.* [Kawczyński *et al.*, 2000; Kawczyński & Strizhak, 2000] and Rachwalska *et al.* [Rachwalska & Kawczyński, 2001] discovered MMO-adding phenomena in a system of three-variable autonomous ordinary differential equations (ODEs) and elucidated that these phenomena occur many times in succession, resembling the period-adding bifurcation in the circle map. Shimizu *et al.* discovered the simplest MMO-adding phenomena denoted by $[1^2, 1^3 \times n]_{n+1}$ for successive n in a forced BVP dynamics and refer to the resulting bifurcations as MMO-incrementing bifurcations (MMOIBs) [Shimizu *et al.*, 2012].

Kousaka *et al.* [2017] investigated the generation of MMOIBs using a constrained BVP oscillator that includes a diode. This constrained BVP oscillator is described with an infinitely large parameter g that corresponds to the ON conductance of the diode. As g tends to infinity, the governing equation is written by a piecewise one-dimensional (1D) nonautonomous equation, and the Poincaré return map is exactly 1D. Using 1D return maps, Kousaka *et al.* [2017] showed that MMOIBs can occur many times in succession and that the limiting ratio of the previous bifurcation parameter interval to the next one between every MMOIB converges to 1. The study of MMOIBs is of great importance because understanding MMOIBs has played a major role in establishing control strategies for chemical reactions and myocardial arrhythmias [Tsumoto *et al.*, 2017]. Engineers and researchers have therefore achieved numerous research results in the fields of medicine, chemistry, and engineering, among others.

In a previous study [Inaba & Kousaka, 2020a], the authors examined these constrained dynamics to elucidate that MMOs can be nested. Namely, between the 1^2- and 1^3-generating regions, simple (un-nested) MMOIBs generate the sequence of $[1^2, 1^3 \times n]_{n+1}$ oscillations for successive n. Nested MMOIBs generate $[[1^2, 1^3 \times 1]_2, [1^2, 1^3 \times 2]_3 \times n]_{3n+2}$ nested MMO sequences for successive n between the regions that generate two adjacent simple MMOIB-generated $[1^2, 1^3 \times 1]_2$ and $[1^2, 1^3 \times 2]_3$ MMOs. Furthermore, we discovered that nested MMOs occur in the classical forced BVP oscillator [Inaba & Tsubone, 2020b]. We imagine that some researchers may already have observed nested MMOIB-generated MMOs because MMOIBs have enjoyed extensive numerical study [Kawczyński *et al.*, 2000; Kawczyński & Strizhak, 2000; Rachwalska & Kawczyński, 2001; Scott, 1993; Shimizu *et al.*, 2012; Shimizu & Inaba, 2016a] and experimental study [Albahadily *et al.*, 1989; Maselko & Swinney, 1986; Shimizu *et al.*, 2015; Shimizu & Inaba, 2016b]. However, these authors may have failed to identify the observed phenomena because such phenomena could be very difficult to understand as

nested MMOIBs without knowing the MMO pattern in advance.

We deduced that nested MMOIBs can generate nested MMO sequences $[[1^2, 1^3 \times m]_{m+1}, [1^2, 1^3 \times (m+1)]_{m+2} \times n]_{(m+2)n+(m+1)}$ for successive integers n and m. This work was limited; however, in that, we confirmed only the case for $m = 1$, and we did not prepare two-parameter bifurcation diagrams.

This paper reports one- and two-parameter bifurcation diagrams and first return maps for the classical BVP oscillator for $m = 1, 2$, and 3. Since the dynamics are slow–fast and the gradient of the nonlinear conductor characteristic $(-x + x^3)$ is very steep for $x > 1$, the first return maps are approximately 1D. The two-parameter bifurcation diagrams are prepared using the shooting algorithm proposed by Kawakami [1984]. These diagrams show that nested MMOIB-generated MMOs appear via saddle-node bifurcations and that period-doubling bifurcations make the MMOs disappear. Because complex bifurcations do not occur in the two-parameter bifurcation diagram, we conclude that nested MMOs are stable. At the level of precision with which we can investigate the one-parameter bifurcation diagrams, we conclude that nested MMOIB-generated MMOs occur successively for $m = 1, 2$, and 3.

This conclusion suggests that in the 30 over years long history of MMO research, several researchers may have been observing time series waveforms of nested MMOs without recognizing their ordered nature, because they appear to be complex at first glance.

The rest of this paper is organized as follows. Section 2 describes the dynamical system of interest in detail. Section 3 then presents and discusses bifurcation diagrams, time series waveforms, and the first return maps to give evidence for the universality and ordered appearance of nested MMOs. Conclusions are drawn in Sec. 4.

2. Circuit Setup

The circuit diagram of the classical forced BVP oscillator is shown in Fig. 1(a). In the figure, x and y are state variables that correspond to the voltage generated across capacitor C and the current flowing through inductor L, respectively. Since the notation L is also used as the number of large excursions in MMOs, we avoid confusion by rescaling the system so that the inductance L is normalized to 1. In the figure, $C = \varepsilon$ is a small parameter and is set to 0.1 throughout the present study. Thus, the dynamics are slow–fast, i.e. x changes quickly and y changes slowly. k_1 is a linear resistor, and B_0 is a DC voltage source, respectively. Furthermore, $g(x)$ is the current flowing through a nonlinear negative-resistance conductor, whose characteristics are represented by the following third-order polynomial function:

$$g(x) = -x + x^3. \tag{1}$$

In the following discussion, normalized variables and parameters are used. Finally, ω and B_1 are the angular frequency and amplitude of the forcing term, respectively, and these are varied as the

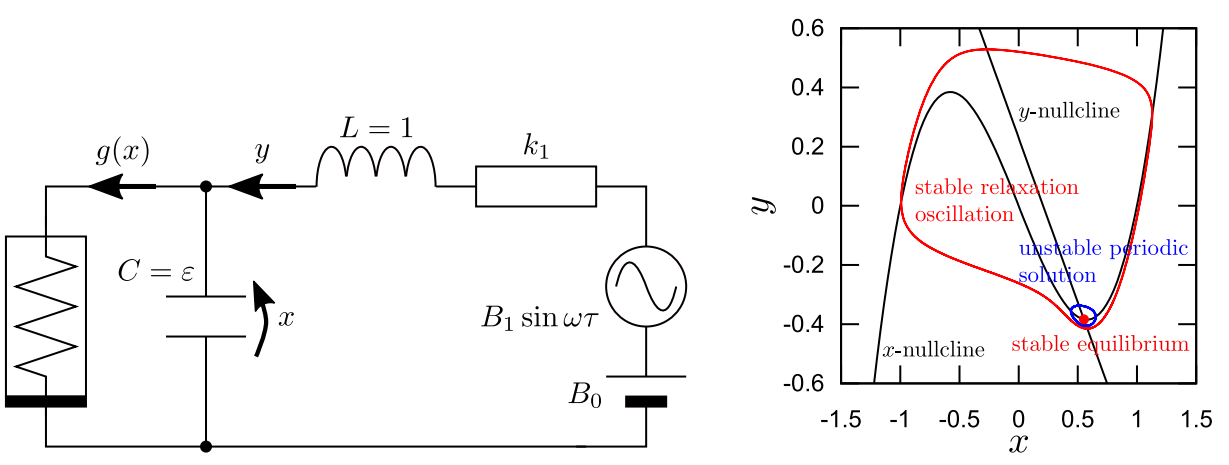

(a) (b)

Fig. 1. (a) Circuit diagram of a forced BVP oscillator near a subcritical Hopf bifurcation point and (b) geometric structure of the (x–y)-plane in the absence of perturbations. Red: stable relaxation oscillation; blue: unstable periodic solution; red bullet: stable equilibrium.

bifurcation parameters. The constant parameters are set to $k_1 = 0.9$ and $B_0 = 0.207$. At these parameter values, a stable equilibrium coexists with a stable relaxation oscillation due to the subcritical Hopf bifurcation in the absence of perturbations. Figure 1(b) shows the $(x$–$y)$-plane in the absence of perturbations where a stable equilibrium, stable relaxation oscillation, unstable periodic oscillation, and x- and y-nullclines are illustrated.

Note that the BVP oscillators belong to the category of natural circuits, because they comprise only two-terminal elements and voltage sources. In two-terminal elements, the voltages generated across the terminals and the currents flowing in the elements play a crucial role in the dynamics, and two-terminal elements never act as analog computers with input and output voltage terminals [Matsumoto *et al.*, 1985]. Because of this structure, such natural circuits are sometimes equivalent to FitzHugh–Nagumo models [FitzHugh, 1961; Nagumo *et al.*, 1962].

The governing equations of the circuit are represented by the following system of two nonautonomous ODEs:

$$\begin{cases} \varepsilon \dot{x} = y - g(x), \\ \dot{y} = -x - k_1 y + B_0 + B_1 \sin \omega\tau \end{cases} \left(\frac{\mathrm{d}}{\mathrm{d}\tau} = \cdot \right). \tag{2}$$

Simple mixed-mode oscillations will arise. To observe behaviors of MMOs precisely in a one-parameter bifurcation diagram, the following subsets are defined:

$$\begin{aligned} \Pi_- &= \{(\tau, x, y) \,|\, x = 1, y - g(x) < 0 (\dot{x} < 0)\}, \\ \Pi_+ &= \{(\tau, x, y) \,|\, x = 1, y - g(x) > 0 (\dot{x} > 0)\}, \\ \Sigma_1 &= \{(\tau, x, y) \,|\, x = 1, y - g(x) = 0 (\dot{x} = 0)\}. \end{aligned} \tag{3}$$

The dynamics of the forced BVP oscillator with vector fields and selected trajectories projected onto a two-dimensional state space are illustrated in Fig. 2.

Let us consider a flow that leaves a point on Π_- just below Σ_1 marked (τ_0, y_0) in Fig. 2(a). The solution leaving Π_- enters the $x < 1$ region and strikes Π_+ at a positive time at a point marked P in the figure. Then, the solution passes along the x-nullcline in the $x > 1$ region, as shown in Fig. 2(b) and strikes Π_- again at the point marked (τ_1, y_1) in Fig. 2(a), close to Σ_1. y_1 is close to 0 because of the slow–fast dynamics, and the gradient of $g(x)$ is very steep for $x > 1$ since ε is small. Therefore $y - g(x) \simeq 0$ when x is slow.

A global view of the one-parameter bifurcation diagram between the 1^2- and 1^3-MMO generating regions is shown in Fig. 3(a). The bifurcation parameter B_1 is set to 0.0105. $\theta_k = \omega\tau_k/2\pi$ mod 1 for large k is plotted in Figs. 3(a) and 3(b). Figure 3(a) was created using the continuous deformation method, which is standard for preparing one-parameter bifurcation diagrams. The continuous deformation method uses the following steps. Let T be a Poincaré return map defined on plane Π_-. Let M and N be sufficiently large integers. In

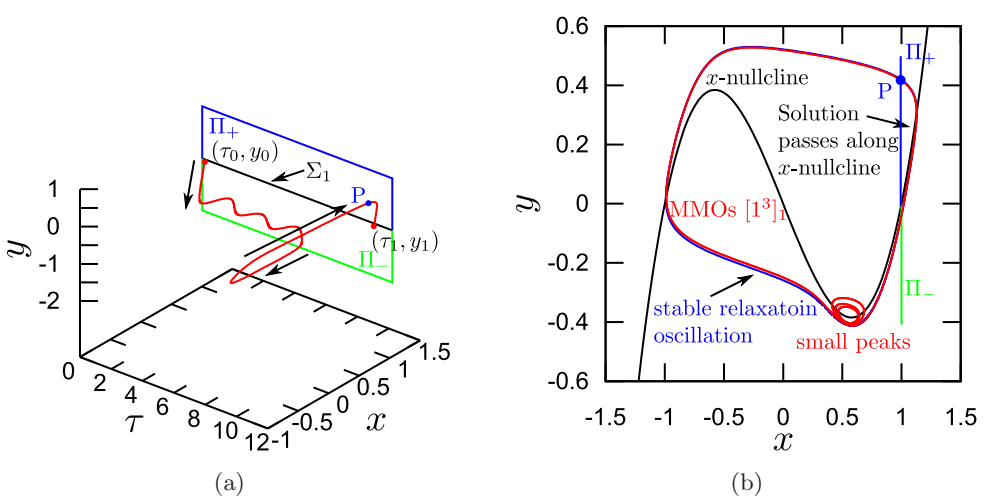

(a) (b)

Fig. 2. (a) Geometric structure of the vector fields and (b) projection of x-nullcline, relaxation oscillation, Π_-, Π_+, and $[1^3]_1$ solution onto the $(x$–$y)$-state space. Black: x-nullcline; blue: stable relaxation oscillation; red: $[1^3]_1$ MMO trajectory; light green: Π_-; blue: Π_+.

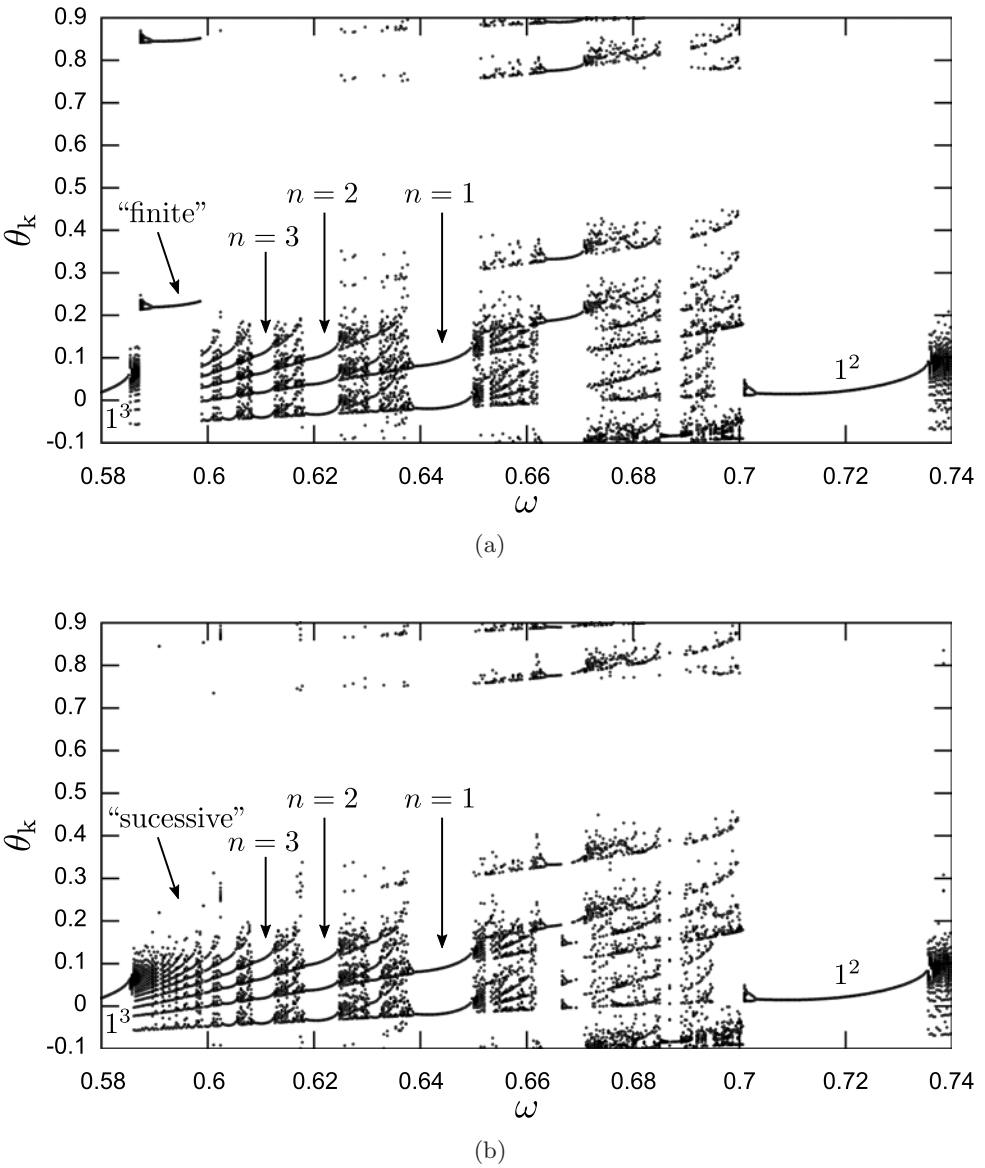

Fig. 3. One-parameter bifurcation diagram for $B_1 = 0.0105$ where MMOIB-generated $[1^2, 1^3 \times n]_{n+1}$ MMOs appear using (a) the continuous deformation method and (b) fixed initial conditions $(\tau_0, x_0, y_0) = (0.1(2\pi/\omega), 1, 0)$. Only finite MMOIBs can be observed in (a), whereas successive MMOIBs appear in (b).

this case, $T^1(\tau_0, y_0)$–$T^M(\tau_0, y_0)$ and $T^{M+1}(\tau_0, y_0)$–$T^{M+N}(\tau_0, y_0)$ at $\omega = \omega_{\text{PRESENT}}$ are the transient and stationary states, respectively. At the next step, $\omega = \omega_{\text{NEXT}} = \omega_{\text{PRESENT}} + \Delta\omega$, where $\Delta\omega$ is sufficiently small, and $T^{M+N}(\tau_0, y_0)$ is used for the initial conditions of T. With this method, most systems will yield smooth one-parameter bifurcation diagrams, but one can see a clear discontinuity in the transition from 1^3 to 1^2 sequences in Fig. 3(a), in the region $0.58 < \omega < 0.6$. This suggests that some of the MMOIBs in this bifurcation diagram are being obfuscated by the continuous deformation method. The transition between MMOs in Fig. 3(a) appears to include regions of chaotic behavior, and the transitions from these chaotic regions to periodic solutions are not guaranteed to be MMOIBs. The missing MMOIBs appear when instead of using the continuous deformation method, we set the initial conditions to $(\tau_0, x_0, y_0) = (0.1(2\pi/\omega), 1, 0)$ as shown in Fig. 3(b). We will discuss the reason for choosing these initial conditions in the next section.

One-dimensional time series waveform of some of the MMOs and MMOIB-generated MMOs that appear between the 1^2- and 1^3-generating regions of the bifurcation diagram are shown in Fig. 4.

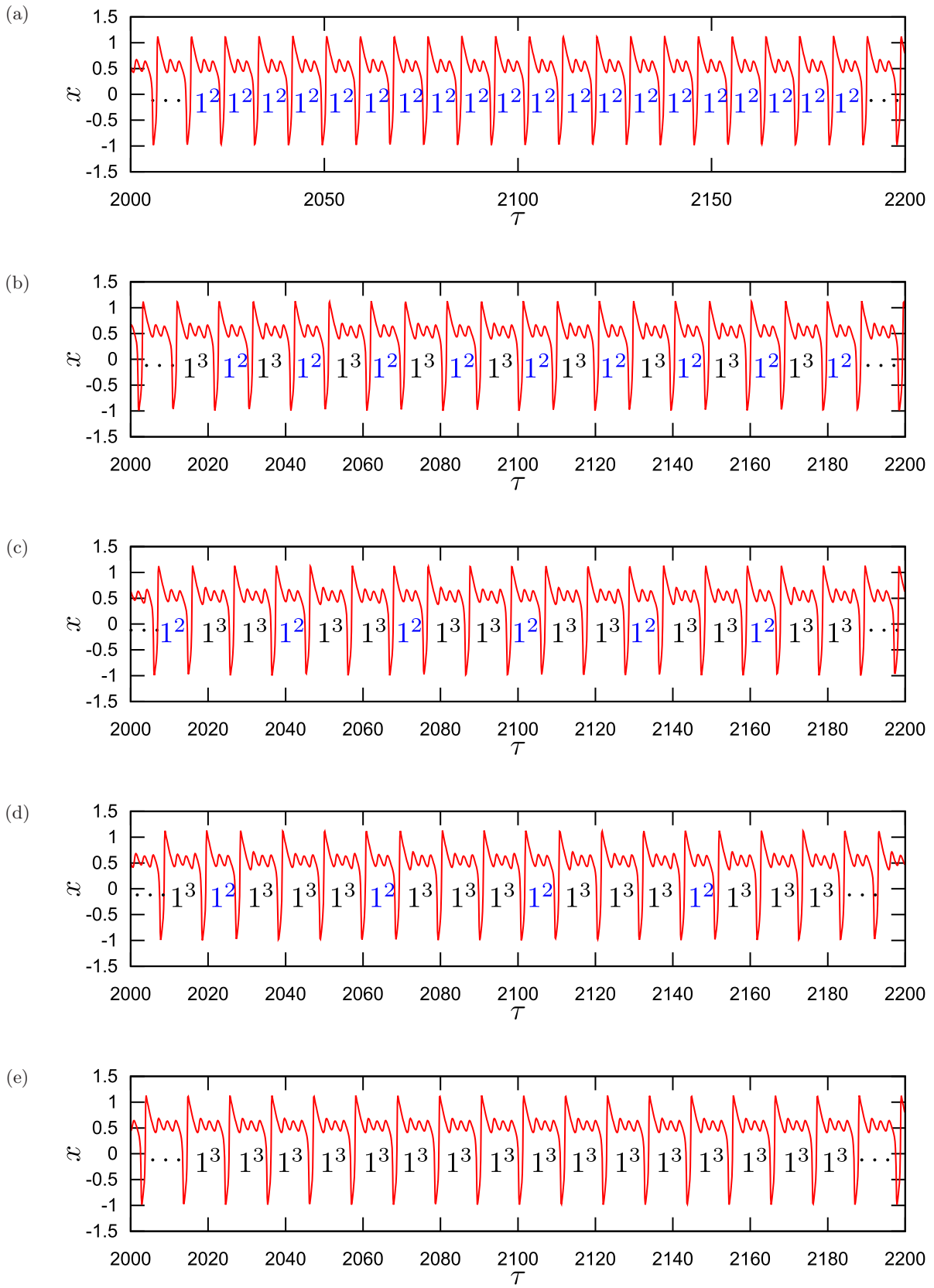

Fig. 4. Simple MMOs and MMOIB-generated MMOs between them in the bifurcation diagram. (a) $[1^2]_1$ for $\omega = 0.72$, (b) $[1^2, 1^3 \times 1]_2$ for $\omega = 0.64$, (c) $[1^2, 1^3 \times 2]_3$ for $\omega = 0.62$, (d) $[1^2, 1^3 \times 3]_4$ for $\omega = 0.61$ and (e) $[1^3]_1$ for $\omega = 0.58$. The initial conditions are fixed to $(\tau_0, x_0, y_0) = (0.1(2\pi/\omega), 1, 0)$. The trigger sequence 1^2 is marked blue.

3. Nested MMOs

When we magnify Fig. 3(b) between two adjacent MMOIB-generated $[1^2, 1^3 \times 1]_2$ and $[1^2, 1^3 \times 2]_3$ MMOs, we observe successive nested MMO sequences that are generated by MMOIBs: $[[1^2, 1^3 \times 1]_2, [1^2, 1^3 \times 2]_3 \times n]_{3n+2}$ for $n = 1, 2, 3$. A zoomed-in view of this region of the bifurcation diagram in Fig. 3(b) is given in Fig. 5. We have referred to the periodic structures delineated with green lines as nested MMOs [Inaba & Kousaka, 2020a; Inaba & Tsubone, 2020b]. In our numerical results, nested MMOIB-generated MMOs appear in all simulations that yield MMOs. The lower panel of Fig. 5 is a two-parameter bifurcation diagram in the $(\omega$–$B_1)$-plane in the neighborhood of $B_1 = 0.0105$. In this two-parameter bifurcation diagram, G^i and I^j indicate saddle-node and period-doubling bifurcation curves, and the superscripts denote the number of periods of the forcing term in each MMO sequence. These bifurcation curves were drawn using the shooting algorithm presented by Kawakami [1984], which is explained in brief in Appendix A. The saddle-node and period-doubling bifurcations indicate the appearance and disappearance of nested MMOIB-generated MMOs. From this two-parameter bifurcation diagram, we can see that nested MMOs exist and remain stable as the parameter B_1 is varied. We judge the nested MMOs as stable because no complex bifurcations are observed in the two-parameter bifurcation diagram.

Time series waveforms of nested MMOIB-generated $[[1^2, 1^3 \times 1]_2, [1^2, 1^3 \times 2]_3 \times n]_{3n+2}$ oscillators for $n = 1, 2, 3, 4, 5$, and 6 are shown in Figs. 6(a)–6(f), respectively. Note that nested MMO attractor for $m = n = 1$ was observed

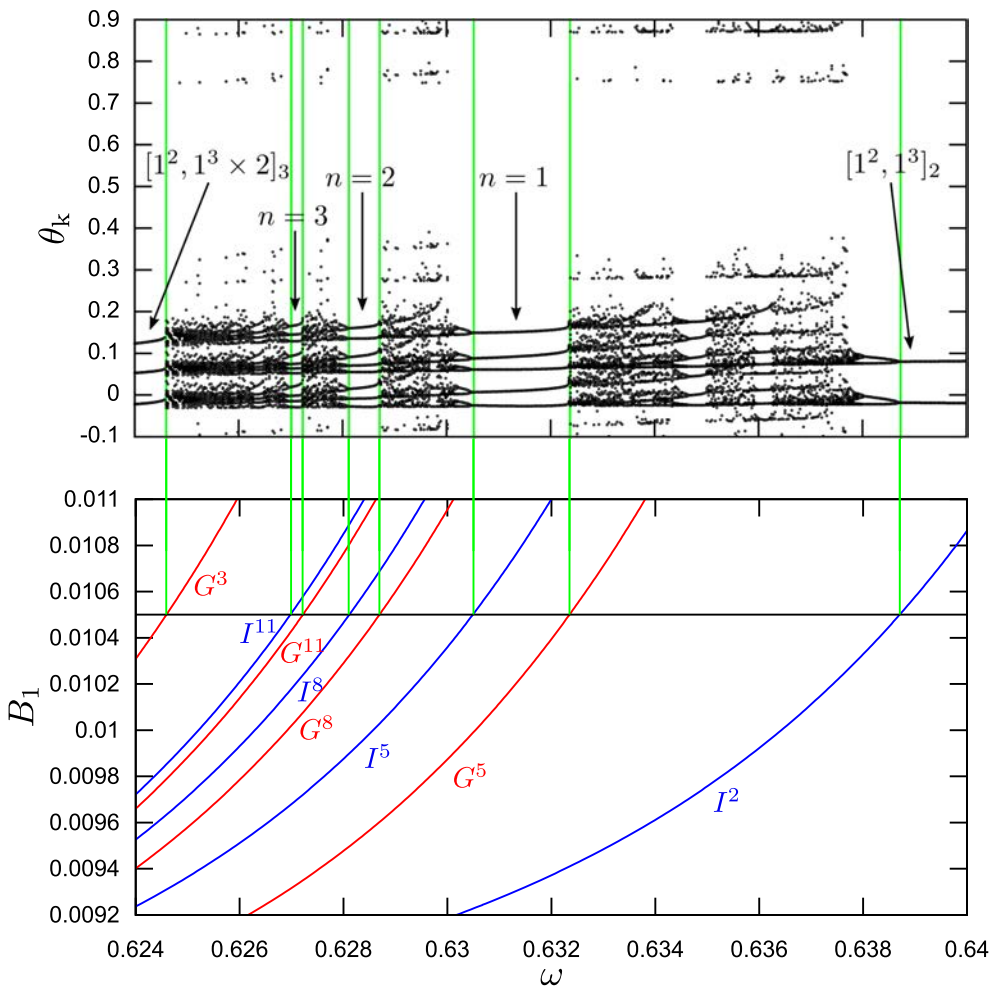

Fig. 5. One-parameter (top panel) and two-parameter (bottom panel) bifurcation diagrams where MMOIB-generated $[[1^2, 1^3 \times 1]_2, [1^2, 1^3 \times 2]_3 \times n]_{3n+2}$ MMOs appear. G^{3n+2} and I^{3n+2} denote saddle-node and period-doubling bifurcations of sets of $3n + 2$-periodic points, respectively.

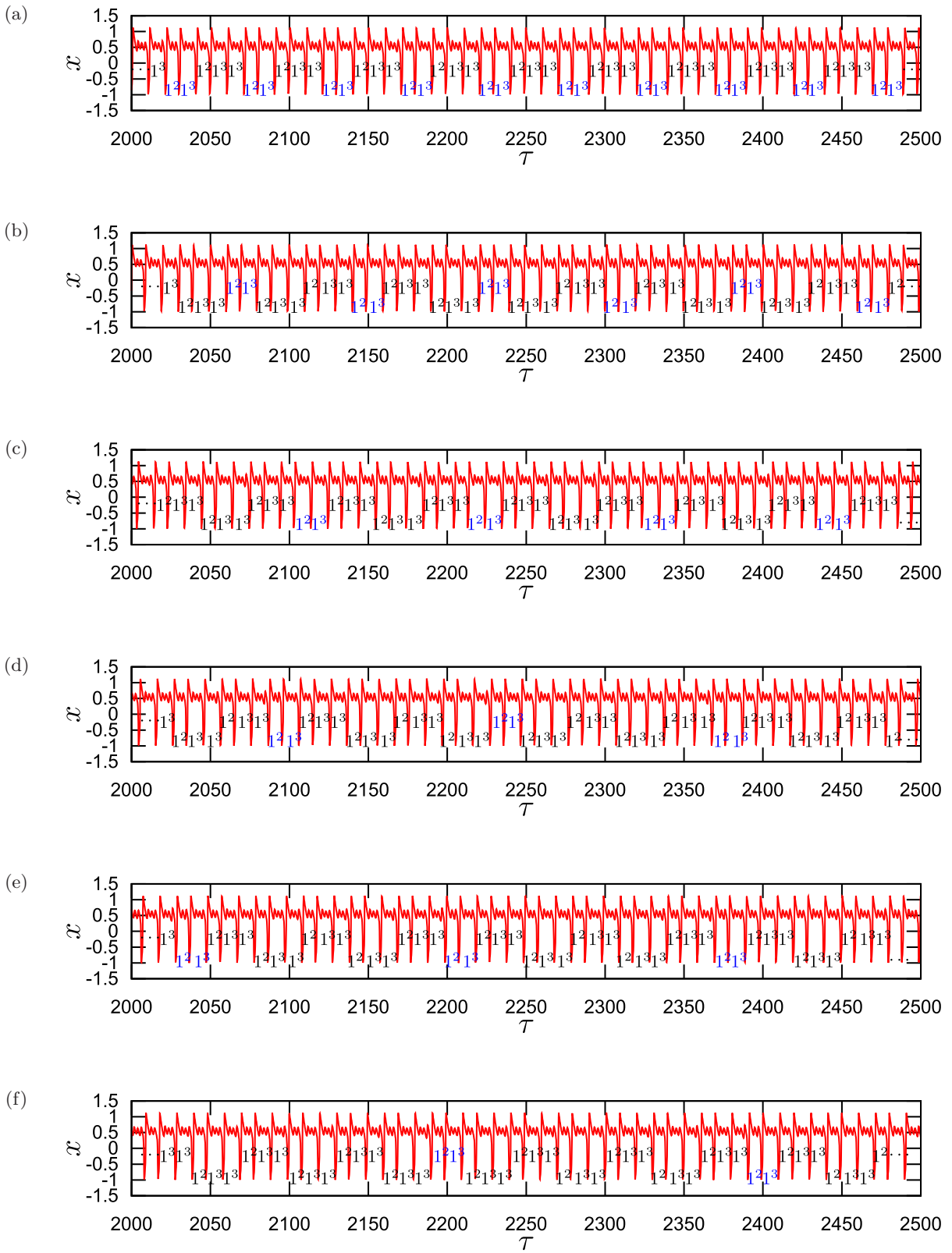

Fig. 6. Time series waveforms of nested MMOIB-generated $[[1^2, 1^3 \times 1]_2, [1^2, 1^3 \times 2]_3 \times n]_{3n+2}$ MMOs, showing (a) $n = 1$ for $\omega = 0.631$, (b) $n = 2$ for $\omega = 0.6284$, (c) $n = 3$ for $\omega = 0.627$, (d) $n = 4$ for $\omega = 0.6264$, (e) $n = 5$ for $\omega = 0.62593$ and (f) $n = 6$ for $\omega = 0.62565$. Fixed initial conditions are used: $(\tau_0, x_0, y_0) = (0.1(2\pi/\omega), 1, 0)$. In these figures, the sequences labeled $1^2 1^3$ in blue in sequences (a)–(f) trigger MMOIB-generated MMOs $[[1^2, 1^3 \times 1]_2, [1^2, 1^3 \times 2]_3 \times n]_{3n+2}$ for $n = 1, 2, 3, 4, 5$, and 6, respectively.

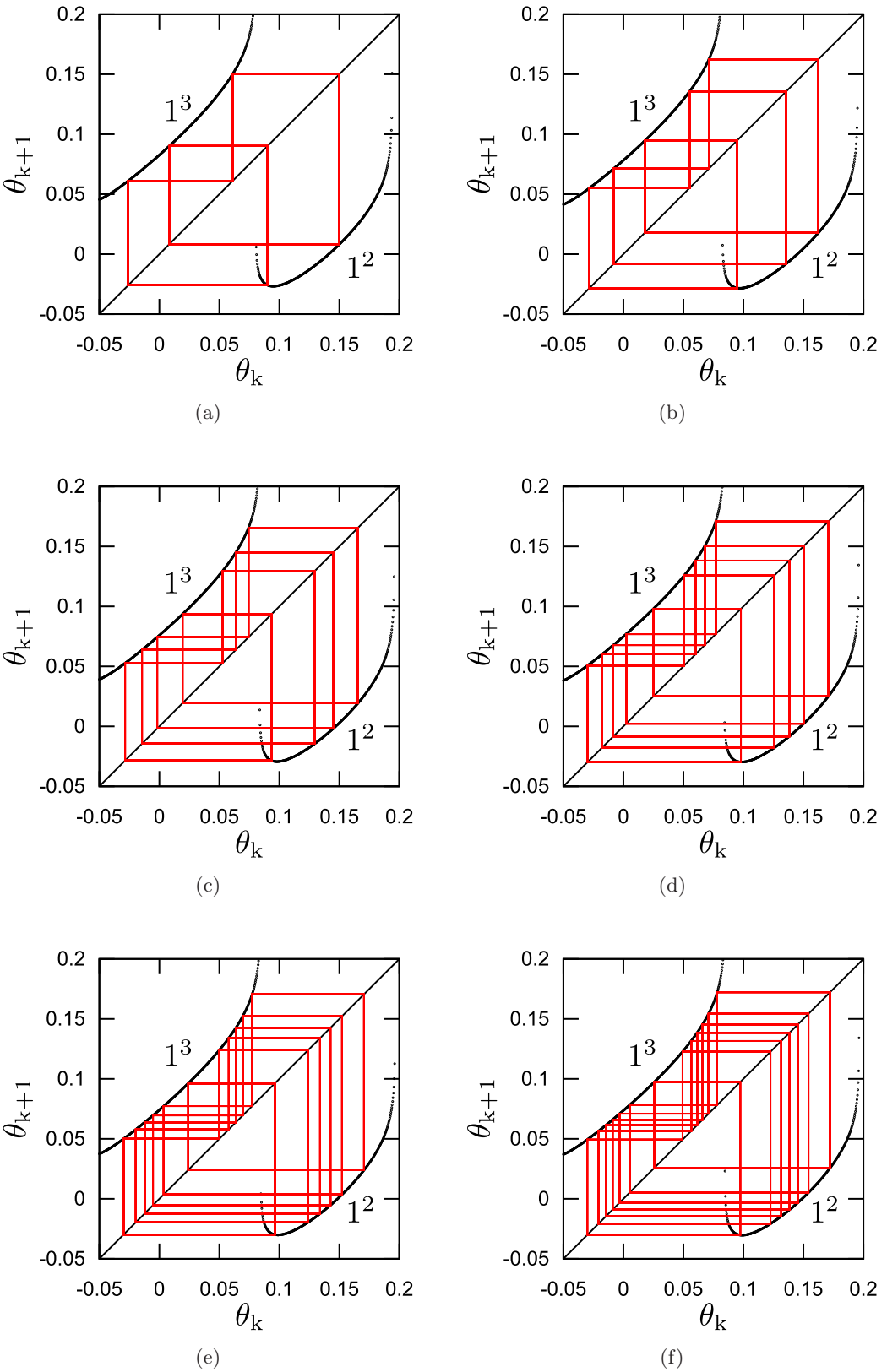

Fig. 7. The first return maps of nested MMOIB-generated MMOs, showing $[[1^2, 1^3]_2, [1^2, 1^3 \times 2]_3 \times n]_{3n+2}$ (a) $n = 1$ for $\omega = 0.631$, (b) $n = 2$ for $\omega = 0.6284$, (c) $n = 3$ for $\omega = 0.627$, (d) $n = 4$ for $\omega = 0.6264$, (e) $n = 5$ for $\omega = 0.62593$ and (f) $n = 6$ for $\omega = 0.62565$.

in experimental measurements [Inaba & Tsubone, 2020b]. The blue symbols denoted by $1^2 1^3$ in Figs. 6(a)–6(f) mark the trigger sequences of nested $[[1^2, 1^3 \times 1]_2, [1^2, 1^3 \times 2]_3 \times n]_{3n+2}$ oscillators for $n = 1, 2, 3, 4, 5$, and 6, respectively. The sequence of nested MMOs follows a surprisingly clear order. However, the sequences of nested MMOs between MMOIBs is difficult to capture even if we do not know the pattern in advance that generates them. It is quite likely that nested MMO time series waveforms have been hiding behind complexity in the last 30 years of results. As shown in Fig. 6, these phenomena are difficult to identify from time series waveforms alone. Note that these are the simplest nested MMO time series waveforms, and they appear quite complex at a glance, although orderly behind the progression of sequences.

As discussed in the previous section, in the plots (τ_0, y_0) and (τ_1, y_1), y_1 takes a value close to 0 because the dynamics are slow–fast and the gradient $g(x)$ is very steep for $x > 1$. Thus, all MMO solutions pass along x-nullcline. This result suggests that first return plots [Inaba & Tsubone, 2020b] will be valuable for distinguishing nested MMOs. Let us consider a flow that leaves $(\tau_0, x_0, y_0) = (\tau_0, 1, 0)$. The solution passes close to an MMO path and returns to $(\tau_1, 1, y_1)$. Note that $y_1 \simeq 0$ as mentioned above. Therefore, the transition from $\theta_0 = \omega\tau_0/2\pi$ to $\theta_1 = \omega\tau_1/2\pi$ mod 1 can be approximated with a one-dimensional map. We call these plots first return maps.

The nested MMOIB-generated MMO trajectories corresponding to $[[1^2, 1^3]_2, [1^2, 1^3 \times 2]_3 \times n]_{3n+2}$ and the corresponding first return maps for $n = 1, 2, 3, 4, 5$, and 6 are shown in Figs. 7(a)–7(f), respectively. The periods of the first return plot trajectories coincide with the number of periods of the forcing term per MMO sequence, i.e. i of G^i or j of I^j. The first return maps clarify the rules by which nested MMOs are ordered. Let us recall that we use fixed initial conditions $(\tau_0, x_0, y_0) = (0.1(2\pi/\omega), 1, 0)$ to create the one-parameter bifurcation diagram. The value $0.1(2\pi/\omega)$ is chosen as the initial time because the first return map passes through a local minimum close to 0.1. Thus, when we use the fixed initial conditions $(\tau_0, x_0, y_0) = (0.1(2\pi/\omega), 1, 0)$, the simulation can track both simple (un-nested) and nested MMOIB-generated MMOs. We presented the trajectories of the first return plots themselves previously [Inaba & Tsubone, 2020b]. The present study introduces approximated first return maps prepared without using constrained dynamics [Kousaka *et al.*, 2017; Inaba & Kousaka, 2020a; Inaba & Tsubone, 2020b] for this system.

The nested MMOIB-generated $[[1^2, 1^3]_2, [1^2, 1^3 \times 2]_3 \times n]_{3n+2}$ MMOs increment and accumulate when n tends to infinity toward the MMO increment-terminating tangent bifurcation point [Kousaka *et al.*, 2017; Inaba & Kousaka, 2020a] at which the $[1^2, 1^3 \times 2]_3$ oscillation emerges. The third-order first return map becomes tangent at three points because the number of the sequence has $[1^2, 1^3 \times 2]_3$ three forcing term. Because this first return map is approximated, the tangent bifurcation point is also derived approximately, and the MMOIB-generated MMO terminates approximately at $\omega = 0.6245911$. The first return map as applied thrice at this point is shown in Fig. 8.

In previous work, we only discussed nested $[[1^2, 1^3 \times m]_{m+1}], [1^2, 1^3 \times (m+1)]_{m+2} \times n]_{(m+2)n+(m+1)}$ MMOs for $m = 1$ [Inaba & Tsubone, 2020b]. In the present study, we confirm the existence of nested MMOIB-generated MMOs for the cases $m = 1, 2$, and 3 using first return maps. Much similar to that depicted in Fig. 5, a two-parameter bifurcation diagram and the corresponding one-parameter bifurcation diagram where nested MMOIB-generated $[[1^2, 1^3 \times 2]_3, [1^2, 1^3 \times 3]_4 \times n]_{4n+3}$ MMOs can be observed for successive n are shown in Fig. 9.

Time series waveforms $[[1^2, 1^3 \times 2]_3, [1^2, 1^3 \times 3]_4 \times n]_{4n+3}$ for $n = 1, 2, 3, 4, 5$, and 6 are shown in Figs. 10(a)–10(f), respectively. This is the case in which $m = 2$. Similarly, the blue symbol denoted by $1^2 1^3 1^3$ $(= [1^2, 1^3 \times 2]_3)$ in Figs. 10(a)–10(f) is the sequence that triggers $[[1^2, 1^3 \times 2]_3, [1^2, 1^3 \times 3]_4 \times n]_{4n+3}$ for $n = 1, 2, 3, 4, 5$, and 6, respectively. As m increases, the time series waveforms of nested MMOIB-generated MMOs become more complicated, as shown in Figs. 10(a)–10(f).

The first return map and the first return plot trajectories corresponding to Figs. 10(a)–10(f) are shown in Figs. 11(a)–11(f), respectively. The first return maps and their plot trajectories allow us to explain nested MMOs well. Similar to Fig. 8, the MMOIB-generated $[[1^2, 1^3 \times 2]_3, [1^2, 1^3 \times 3]_4 \times n]_{4n+3}$ MMO sequences increment and accumulate toward a tangent bifurcation point where $[1^2, 1^3 \times 3]_4$ appears as a consequence of $n \to \infty$. Since the sequence $[1^2, 1^3 \times 3]_4$ has four forcing terms, an approximated first return map applied four times will be tangent to the diagonal line when

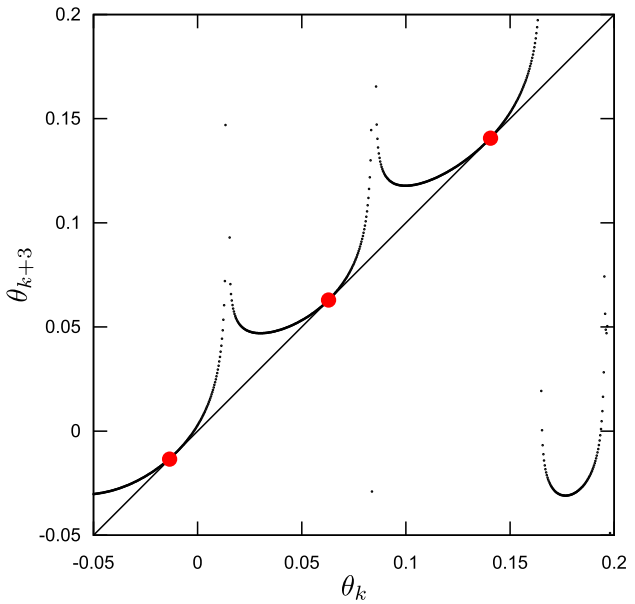

Fig. 8. The shape of first return map applied thrice at the MMO increment-terminating tangent bifurcation point for $\omega = 0.6245911$.

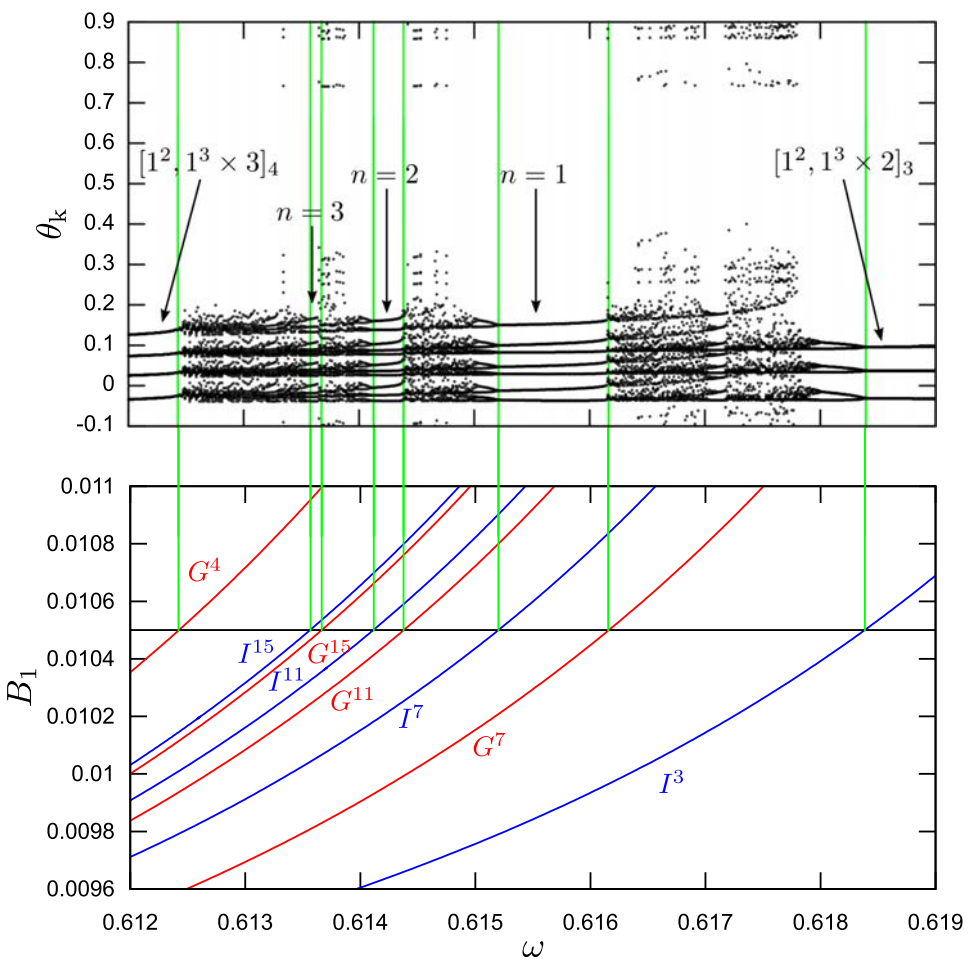

Fig. 9. One-parameter (top panel) and two-parameter (bottom panel) bifurcation diagrams in which MMOIB-generated $[[1^2, 1^3 \times 2]_3, [1^2, 1^3 \times 3]_4 \times n]_{4n+3}$ MMOs appear. G^{4n+3} and I^{4n+3} denote saddle-node and period-doubling bifurcation curves of $4n + 3$-periodic points, respectively.

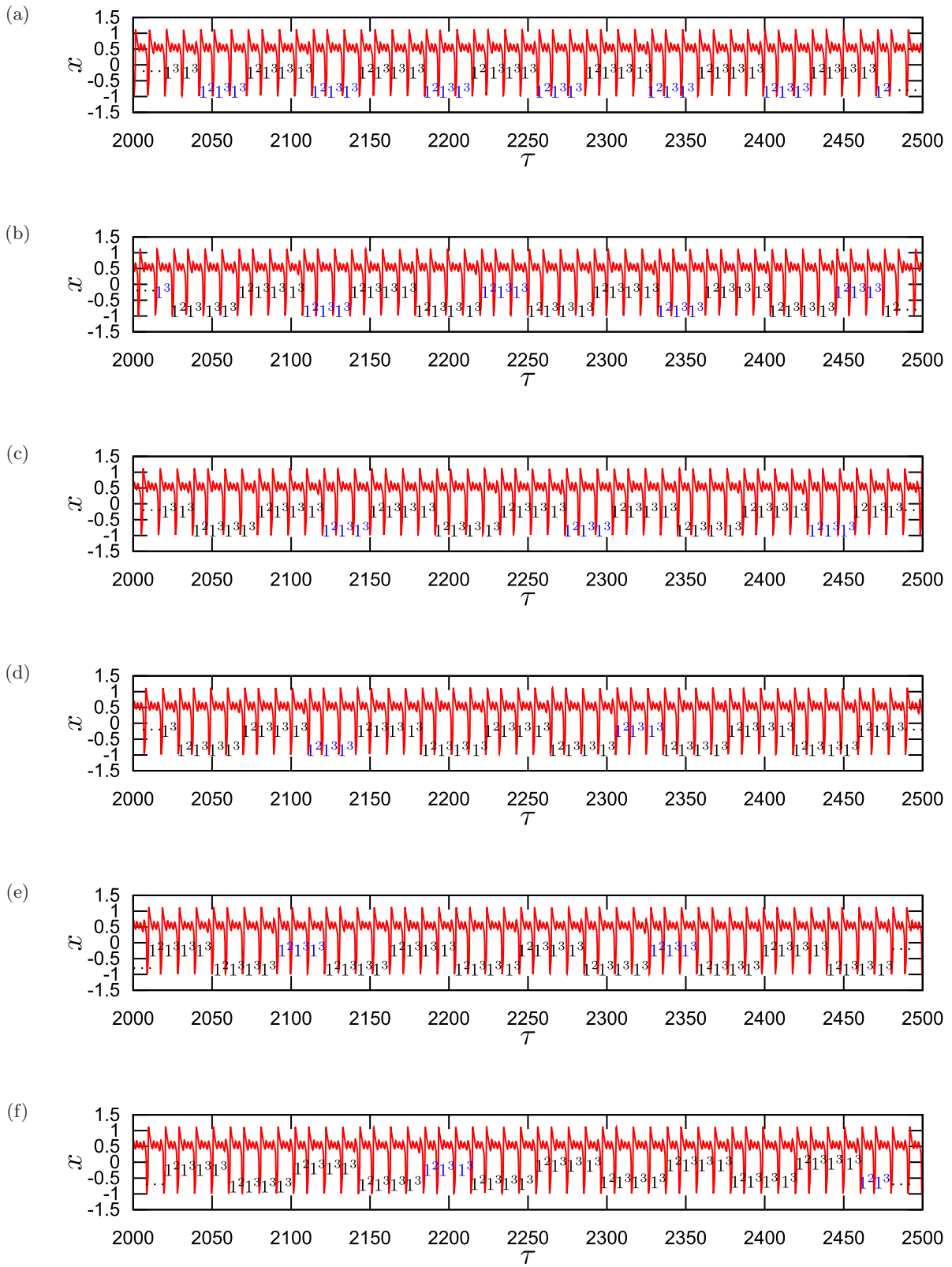

Fig. 10. Time series waveforms of nested MMOIB-generated $[[1^2, 1^3 \times 2]_3, [1^2, 1^3 \times 3]_4 \times n]_{4n+3}$ MMOs, showing (a) $n = 1$ for $\omega = 0.6155$, (b) $n = 2$ for $\omega = 0.6143$, (c) $n = 3$ for $\omega = 0.6136$, (d) $n = 4$ for $\omega = 0.61326$, (e) $n = 5$ for $\omega = 0.61305$ and (f) $n = 6$ for $\omega = 0.61291$. Fixed initial conditions are used: $(\tau_0, x_0, y_0) = (0.1(2\pi/\omega), 1, 0)$. In these figures, the sequences labeled $1^2 1^3 1^3$ in blue in the sequences (a)–(f) trigger MMOIB-generated MMOs $[[1^2, 1^3 \times 2]_3, [1^2, 1^3 \times 3]_4 \times n]_{4n+3}$ for $n = 1, 2, 3, 4, 5$, and 6, respectively.

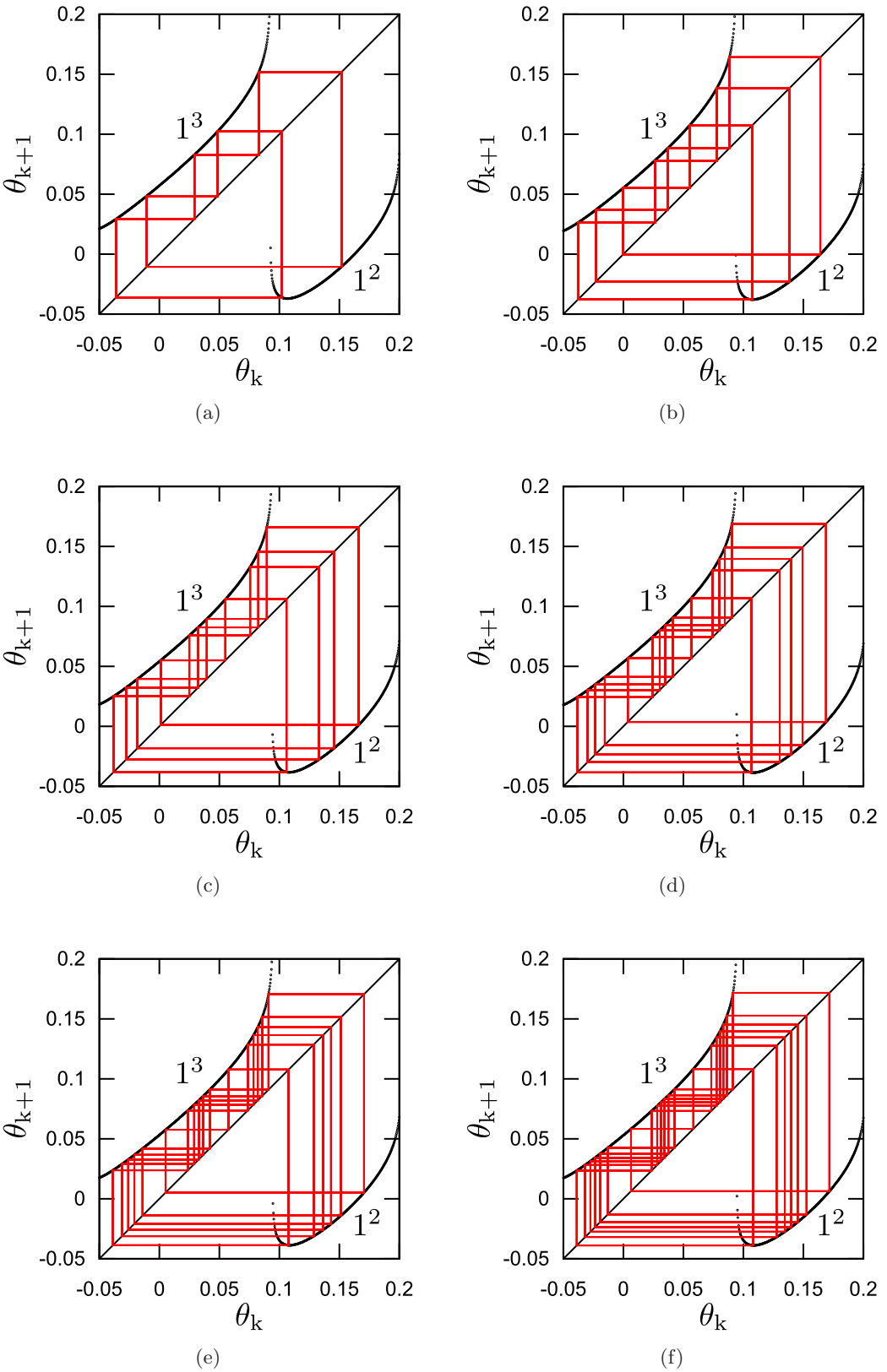

Fig. 11. The first return maps of nested MMOIB-generated MMOs, showing $[[1^2, 1^3 \times 2]_3, [1^2, 1^3 \times 3]_4 \times n]_{4n+3}$ (a) $n = 1$ for $\omega = 0.6155$, (b) $n = 2$ for $\omega = 0.6143$, (c) $n = 3$ for $\omega = 0.6136$, (d) $n = 4$ for $\omega = 0.61326$, (e) $n = 5$ for $\omega = 0.61305$ and (f) $n = 6$ for $\omega = 0.61291$.

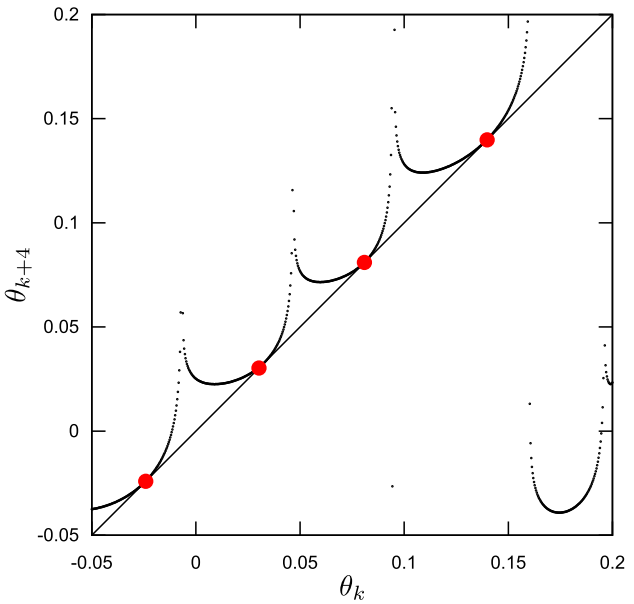

Fig. 12. The shape of the first return map applied four times for $\omega = 0.6124231$.

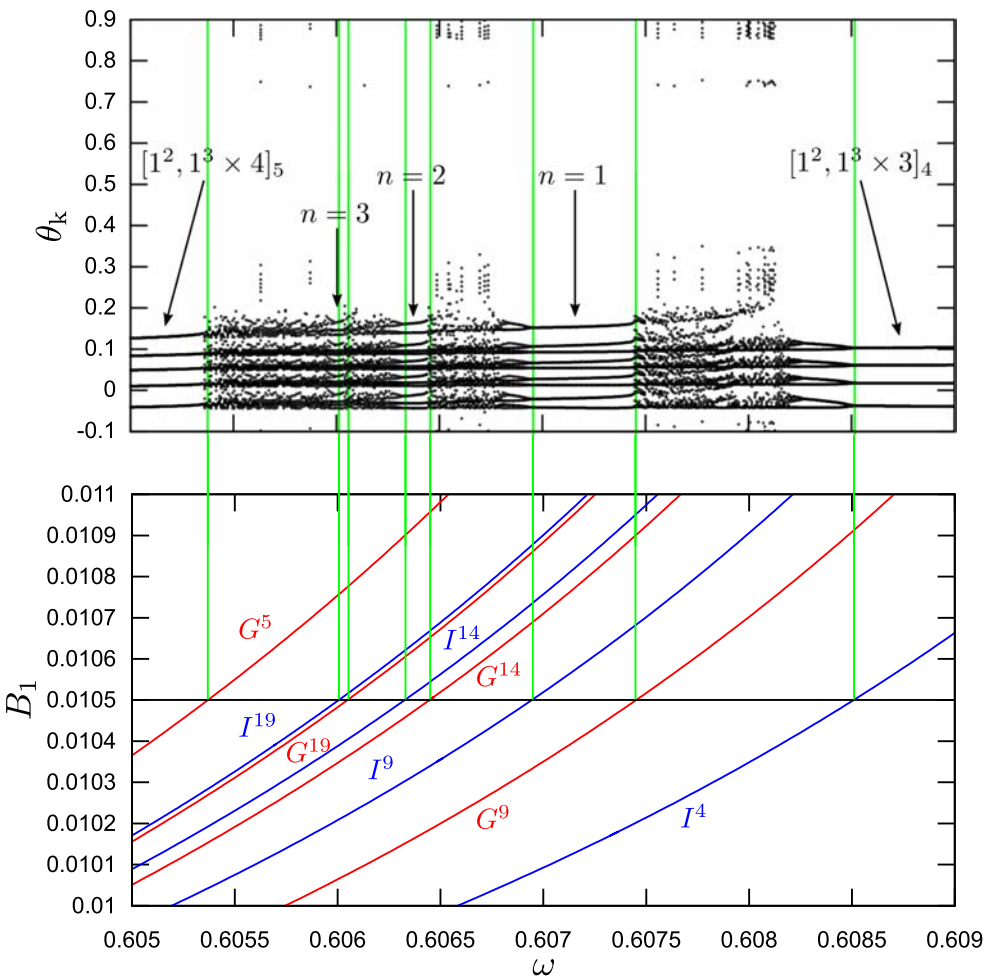

Fig. 13. One-parameter (top panel) and two-parameter (bottom panel) bifurcation diagrams where MMOIB-generated $[[1^2, 1^3 \times 3]_4, [1^2, 1^3 \times 4]_5 \times n]_{5n+4}$ MMOs appear. G_{5n+4} and I_{5n+4} denote saddle-node and period-doubling bifurcation curves of $5n + 4$-periodic points, respectively.

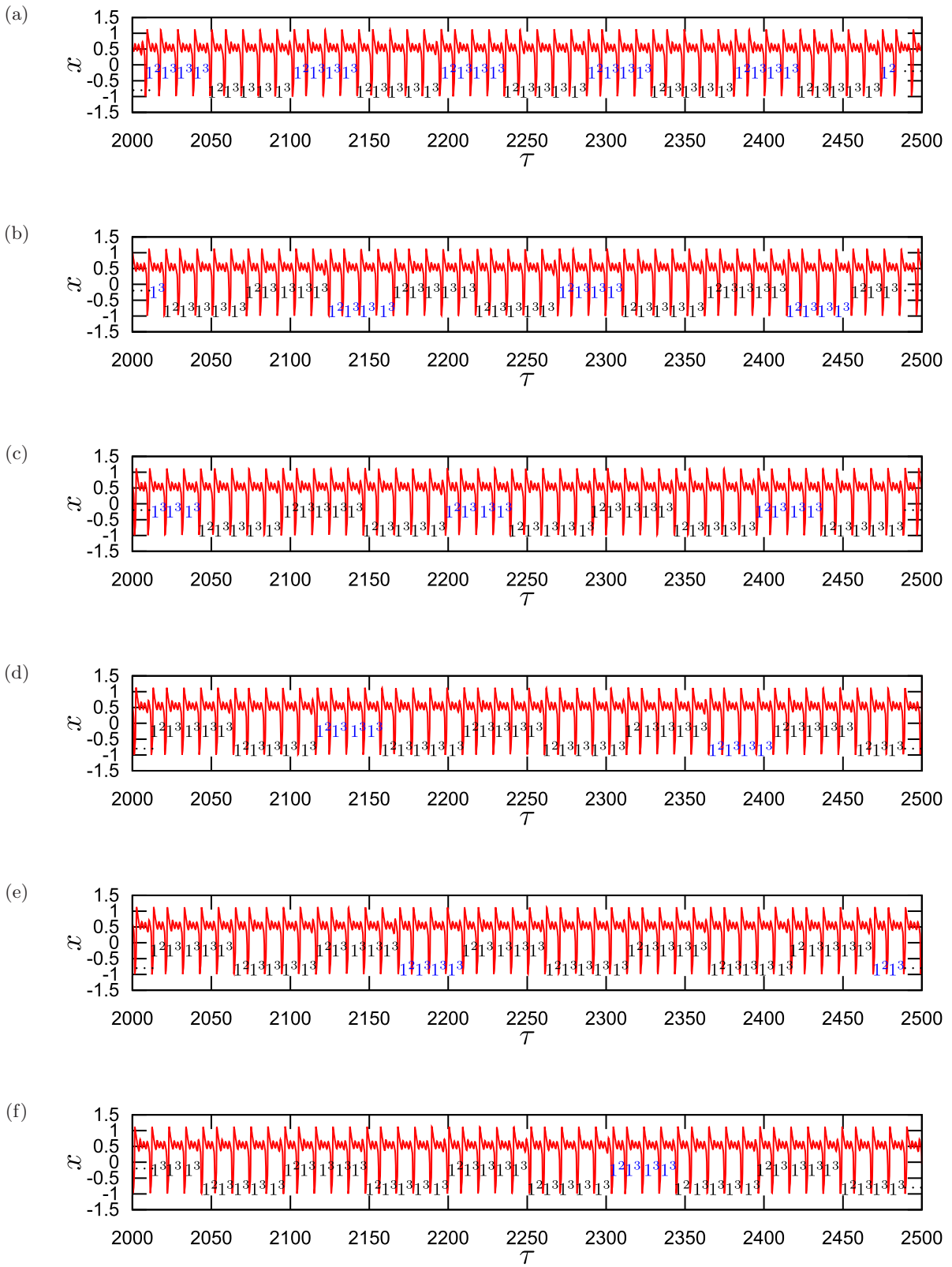

Fig. 14. Time series waveforms of nested MMOIB-generated $[[1^2, 1^3 \times 3]_4, [1^2, 1^3 \times 4]_5 \times n]_{5n+4}$ MMOs, showing (a) $n = 1$ for $\omega = 0.607$, (b) $n = 2$ for $\omega = 0.6064$, (c) $n = 3$ for $\omega = 0.60601$, (d) $n = 4$ for $\omega = 0.60582$, (e) $n = 5$ for $\omega = 0.6057$ and (f) $n = 6$ for $\omega = 0.605625$. Fixed initial conditions $(\tau_0, x_0, y_0) = (0.1(2\pi/\omega), 1, 0)$ are used. In these figures, the sequence labeled $1^2 1^3 1^3 1^3$ in blue in the sequences (a)–(f) trigger MMOIB-generated MMOs $[[1^2, 1^3 \times 3]_2, [1^2, 1^3 \times 4]_5 \times n]_{5n+4}$ for $n = 1, 2, 3, 4, 5$, and 6, respectively.

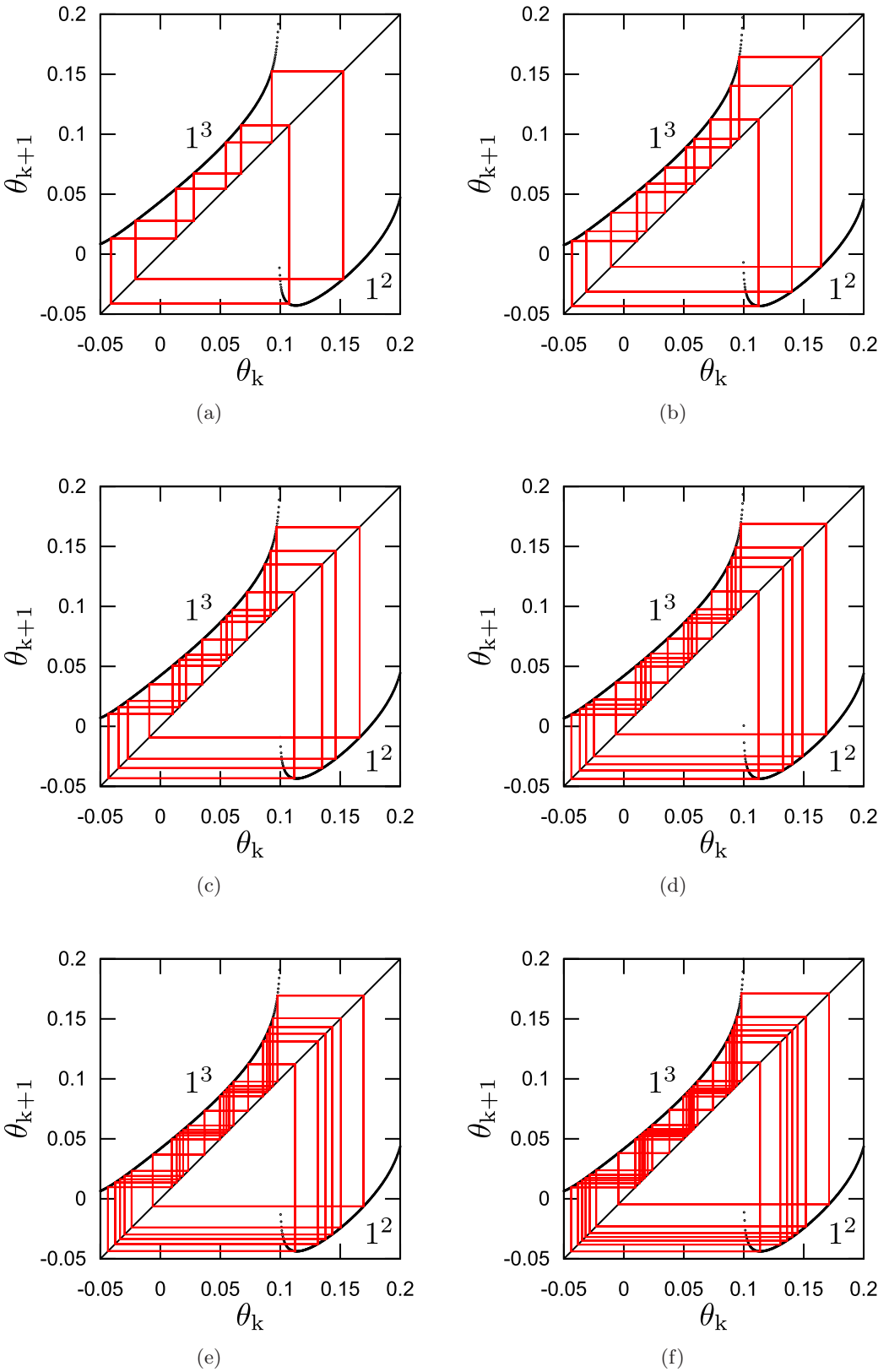

Fig. 15. The first return maps of nested MMOIB-generated MMOs, showing $[[1^2, 1^3 \times 3]_4, [1^2, 1^3 \times 4]_5 \times 1]_{5n+4}$ (a) $n = 1$ for $\omega = 0.607$, (b) $n = 2$ for $\omega = 0.6064$, (c) $n = 3$ for $\omega = 0.60601$, (d) $n = 4$ for $\omega = 0.60582$, (e) $n = 5$ for $\omega = 0.6057$ and (f) $n = 6$ for $\omega = 0.605625$.

n tends to infinity. The point at which the MMO increments terminate is calculated as $\omega = 0.6124231$ when the first return map becomes tangent to the diagonal line after four iterations. The corresponding first return map applied four times is given in Fig. 12.

Two- and one-parameter bifurcation diagrams between the $[1^2, 1^3 \times 3]_4$ and $[1^2, 1^3 \times 4]_5$ MMO-generating regions where nested MMOIB-generated $[[1^2, 1^3 \times 3]_4, [1^2, 1^3 \times 4]_5 \times n]_{5n+4}$ MMOs emerge for successive n are shown in Fig. 13. The time series waveforms corresponding to $[[1^2, 1^3 \times 3]_4, [1^2, 1^3 \times 4]_5 \times n]_{5n+4}$ for $n = 1, 2, 3, 4, 5$, and 6, respectively, are shown in Figs. 14(a)–14(f). Similar to the figures above, the blue symbol denoted by $1^2 1^3 1^3 1^3$ in Figs. 14(a)–14(f) is the trigger sequence of $[[1^2, 1^3 \times 3]_4, [1^2, 1^3 \times 4]_5 \times n]_{5n+4}$ for $n = 1$, $2, 3, 4, 5$, and 6, respectively. Finally, the corresponding first return maps and their trajectories are shown in Figs. 15(a)–15(f). Even if the first return maps are applied, distinguishing between $[[1^2, 1^3 \times 3]_4, [1^2, 1^3 \times 4]_5 \times n]_{5n+4}$ with $n = 5$ and $n = 6$ is difficult because the period of the first return plots is already 34. However, the MMO increment-terminating tangent bifurcation point can be easily derived if we apply the condition that $[1^2, 1^3 \times 4]_5$ emerges as a consequence of $[[1^2, 1^3 \times 3]_4, [1^2, 1^3 \times 4]_5 \times n]_{5n+4}$ for $n \to \infty$. In this case, the first return map applied five times becomes tangent to the diagonal line at the bifurcation point.

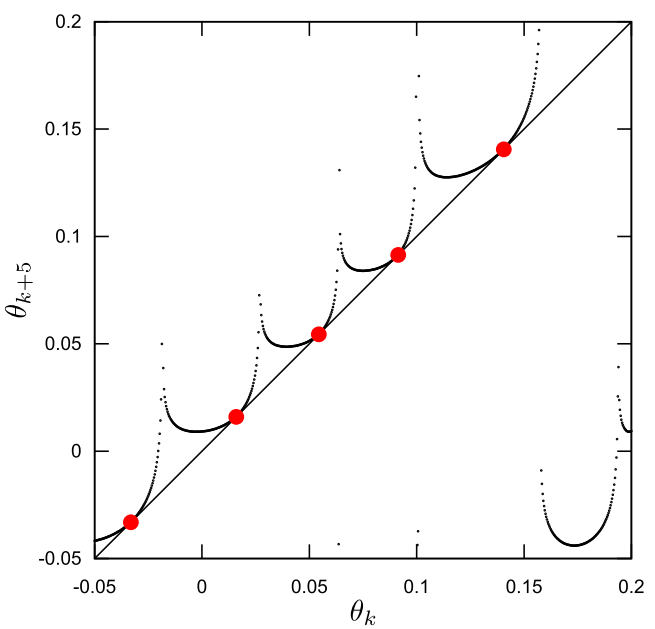

Fig. 16. The shape of the first return map applied four times for $\omega = 0.605369$.

The MMO increment-terminating tangent bifurcation point can be approximately derived under these conditions as $\omega = 0.605369$ (see Fig. 16). Therefore, our numerical results indicate that nested MMOs are universal phenomena because they are strongly ordered and can be observed for successively increasing values of m, which is one of the values of successive n of simple (un-nested) MMOIBs.

4. Conclusion

We investigated nested MMOs generated by a classical forced BVP oscillator in which the nonlinear term is expressed as a third-order polynomial function. Numerical methods were used to prepare three magnified views of this system's global one-parameter bifurcation diagram. Each of the three diagrams resembles the global view, indicating that self-similar structures can exist in chaotic windows. The nested MMOIB-generated MMOs are judged to be stable because the bifurcation structures of the two-parameter bifurcation diagrams remain unchanged. Furthermore, we defined approximated first return maps and used these to confirm that nested MMOIB-generated MMOs are explained well by the rules we have fomulated. We also used these first return maps to identify the thresholds of the bifurcation parameters at which the MMO increments are terminated by tangent bifurcations.

Acknowledgment

This work was supported by JSPS KAKENHI Grant Numbers JP18K11460 and JP19K12144.

References

Albahadily, F. N., Ringland, J. & Schell, M. [1989] "Mixed-mode oscillations in an electrochemical system. I. A Farey sequence which does not occur on a torus," *J. Chem. Phys.* **90**, 813–821.

Arnol'd, V. I. (ed.) [1994] *Encyclopedia of Mathematical Sciences*, Vol. 5 (Springer-Verlag).

Baer, S. M. & Erneux, T. [1986] "Singular Hopf bifurcation to relaxation oscillations," *SIAM J. Appl. Math.* **46**, 721–739.

Baer, S. M. & Erneux, T. [1992] "Singular Hopf bifurcation to relaxation oscillations. II," *SIAM J. Appl. Math.* **52**, 1651–1664.

Benoit, E., Callot, J. F., Diener, F. & Diener, M. [1981] "Chasse au canard," *Collect. Math.* **31–32**, 37–119.

Braaksma, B. & Grasman, J. [1993] "Critical dynamics of the Bonhoeffer–Van der Pol equation and its chaotic response to periodic stimulation," *Physica D* **68**, 265–280.

Brøns, M., Gross, P. & Bar-Eli, K. [1997] "Circle maps and the devil's staircase in a periodically perturbed Oregonator," *Int. J. Bifurcation and Chaos* **11**, 2621–2628.

Brøns, M., Krupa, M. & Wechselberger, M. [2006] "Mixed mode oscillations due to the generalized canard phenomenon," *Fields Inst. Commun.* **49**, 39–63.

Brøns, M., Kaper, T. J. & Rotstein, H. G. [2008] "Introduction to focus issue: Mixed mode oscillations: Experiment, computation, and analysis," *Chaos* **18**, 015101-1–4.

De Maesschalck, P., Kutafina, E. & Popović, N. [2014] "Three time-scales in an extended Bonhoeffer–van der Pol oscillator," *J. Dyn. Diff. Eqs.* **26**, 955–987.

Desroches, M., Guckenheimer, J., Krauskopf, B., Kuehn, C., Osinga, H. M. & Wechselberger, M. [2012] "Mixed-mode oscillations with multiple time scales," *SIAM Rev.* **54**, 211–288.

Desroches, M., Kaper, T. J. & Krupa, M. [2013] "Mixed-mode bursting oscillations: Dynamics created by a slow passage through spike-adding canard explosion in a square-wave burster," *Chaos* **23**, 046106.

Diener, M. [1984] "The canard unchained or how fast/slow dynamical problems bifurcate," *Math. Intell.* **6**, 38–49.

FitzHugh, R. [1961] "Impulses and physiological states in theoretical models of nerve membrane," *Biophys. J.* **1**, 445–466.

Freire, J. G. & Gallas, J. A. C. [2011a] "Stern-Brocot trees in cascades of mixed-mode oscillations and canards in the extended Bonhoeffer–van der Pol and the FitzHugh–Nagumo models of excitable systems," *Phys. Lett. A* **375**, 1097–1103.

Freire, J. G. & Gallas, J. A. C. [2011b] "Stern-Brocot trees in the periodicity of mixed-mode oscillations," *Phys. Chem. Chem. Phys.* **13**, 12101–12336.

Guckenheimer, J., Hoffman, K. & Weckesser, W. [2000] "Numerical computation of canards," *Int. J. Bifurcation and Chaos* **10**, 2669–2687.

Guckenheimer, J. & Scheper, C. [2011] "A geometric model for mixed-mode oscillations in a chemical system," *SIAM J. Appl. Dyn. Syst.* **10**, 92–128.

Hudson, J. L., Hart, M. & Marinko, D. [1979] "An experimental study of multiple peak periodic and nonperiodic oscillations in the Belousov–Zhabotinskii reaction," *J. Chem. Phys.* **71**, 1601–1606.

Inaba, N. & Kousaka T. [2020a] "Nested mixed-mode oscillations," *Physica D* **401**, 132152-1–18.

Inaba, N. & Tadashi T. [2020b] "Nested mixed-mode oscillations, part II: Experimental and numerical study of a classical Bonhoeffer–van der Pol oscillator," *Physica D* **406**, 132493-1–29.

Itoh, M. & Tomiyasu, R. [1990] "Experimental study of the missing solutions "canards"," *IEICE Trans.* **E73**, 848–854.

Kawakami, H. [1984] "Bifurcation of periodic responses in forced dynamic nonlinear circuits: Computation of bifurcation values of the system parameters," *IEEE Trans. Circuits Syst.* **31**, 248–260.

Kawczyński, A. L. & Strizhak, P. E. [2000] "Period adding and broken Farey tree sequences of bifurcations for mixed-mode oscillations and chaos in the simplest three-variable nonlinear system," *J. Chem. Phys.* **112**, 6122–6130.

Kawczyński, A. L., Khavrus, V. O. & Strizhak, P. E. [2000] "Complex mixed-mode periodic and chaotic oscillations in a simple three-variable model of nonlinear system," *Chaos* **10**, 299–310.

Kousaka, T., Ogura, Y., Shimizu, K., Asahara, H. & Inaba, N. [2017] "Analysis of mixed-mode oscillation-incrementing bifurcations generated in a nonautonomous constrained Bonhoeffer–van der Pol oscillator," *Physica D* **353–354**, 48–57.

Krupa, M., Popović, N. & Kopel, N. [2008] "Mixed-mode oscillations in three time-scale systems: A prototypical example," *SIAM J. Appl. Dyn. Syst.* **7**, 361–420.

Kuehn, C. [2015] *Multiple Time Scale Dynamics* (Springer International Publishing).

Kutafina, E. [2015] "Mixed mode oscillations in the Bonhoeffer–van der Pol oscillator with weak periodic perturbation," *Comput. Appl. Math.* **34**, 81–92.

Markman, G. & Bar-Eli, K. [1994] "Periodic perturbations of an oscillatory chemical system," *J. Chem. Phys.* **98**, 12248–12254.

Maselko, J. & Swinney, H. L. [1986] "Complex periodic oscillations and Farey arithmetic in the Belousov–Zhabotinskii reaction," *J. Chem. Phys.* **85**, 6430–6441.

Matsumoto, T., Chua, L. O. & Komuro, M. [1985] "The double scroll," *IEEE Trans. Circuits Syst.* **32**, 798–818.

Muratov, C. B. & Vanden-Eijnden, E. [2008] "Noise-induced mixed-mode oscillations in a relaxation oscillator near the onset of a limit cycle," *Chaos* **18**, 015111.

Nagumo, J., Animoto, S. & Yoshizawa, S. [1962] "An active pulse transmission line simulating nerve axon," *Proc. Inst. Radio Engin.* **50**, 2061–2070.

Orban, M. & Epstein, I. R. [1982] "Complex periodic and aperiodic oscillation in the Chlorite–Thiosulfate reaction," *J. Phys. Chem.* **86**, 3907–3910.

Petrov, V., Scott, S. K. & Showalter, K. [1992] "Mixed-mode oscillations in chemical systems," *J. Chem. Phys.* **97**, 6191–6198.

Rachwalska, M. & Kawczyński, A. L. [2001] "Period-adding bifurcations in mixed-mode oscillations in the Belousov–Zhabotinsky reactions at various residence times in a CSTR," *J. Phys. Chem.* **105**, 7885–7888.

Ryashko, L. [2018] "Sensitivity analysis of the noise-induced oscillatory multistability in Higgins model of glycolysis," *Chaos* **28**, 033602.

Scott, S. K. [1993] *Chemical Chaos* (Oxford University Press).

Sekikawa, M., Inaba, N., Yoshinaga, T. & Hikihara, T. [2010] "Period-doubling cascades of canards from the extended Bonhoeffer–van der Pol oscillator," *Phys. Lett. A* **374**, 3745–3751.

Shimizu, K., Sekikawa, M. & Inaba, N. [2011] "Mixed-mode oscillations and chaos from a simple second-order oscillator under weak periodic perturbation," *Phys. Lett. A* **375**, 1566–1569.

Shimizu, K., Saito, Y., Sekikawa, M. & Inaba, N. [2012] "Complex mixed-mode oscillations in a Bonhoeffer–van der Pol oscillator under weak periodic perturbation," *Physica D* **241**, 1518–1526.

Shimizu, K., Sekikawa, M. & Inaba, N. [2015] "Experimental study of complex mixed-mode oscillations generated in a Bonhoeffer–van der Pol oscillator under weak periodic perturbation," *Chaos* **25**, 023105-1–8.

Shimizu, K. & Inaba, N. [2016a] "Piecewise-linear Bonhoeffer–van der Pol dynamics explaining mixed-mode oscillation-incrementing bifurcations," *Prog. Theor. Exp. Phys.* **2016**, 033A01-1–15.

Shimizu, K. & Inaba, N. [2016b] "Experimental and numerical observation of successive mixed-mode oscillation-incrementing bifurcations in an extended Bonhoeffer–van der Pol oscillator," *Int. J. Bifurcation and Chaos* **28**, 1830047-1–10.

Sudhu, S. & Kuehn, C. [2018] "Stochastic mixed-mode oscillations in a three-species predator–prey model," *Chaos* **28**, 033606.

Takahashi, H., Kousaka, T., Asahara, H., Stankevich, N. & Inaba, N. [2018] "Mixed-mode oscillation-incrementing bifurcations and a devil's staircase from a nonautonomous, constrained Bonhoeffer–van der Pol oscillator," *Prog. Theor. Exp. Phys.* **2018**, 103A02-1–16.

Tsumoto, K., Kurata, Y., Furutani, K. & Kurachi, Y. [2017] "Hysteretic dynamics of multi-stable early after depolarisations with repolarisation reserve attenuation: A potential dynamical mechanism for cardiac arrhythmias," *Sci. Rep.* **7**, 10771-1–12.

Yoshinaga, T., Kawakami, K. & Yoshikawa, K. [1988] "A circuit metaphor for nonlinear oscillation in a chemical system at a water-oil interface," *IEICE Trans.* **J71-A**, 1843–1851 (in Japanese).

Zvonkin, A. K. & Shubin, M. A. [1984] "Non-standard analysis and singular perturbations of ordinary differential equations," *Russ. Math. Surv.* **39**, 69–131.

Appendix A

Calculating Bifurcation Parameter Values

This Appendix gives a brief explanation of Kawakami's shooting algorithm for obtaining bifurcation boundary curves [Kawakami, 1984]. Let Eq. (2) be expressed as

$$\dot{\mathbf{x}} = f(\tau, \mathbf{x}), \tag{A.1}$$

where $\mathbf{x} = (x, y)^\top$. Let the Poincaré return map be expressed by T_λ instead of a simple T to indicate that T depends on the bifurcation parameter λ. Let us then define a stroboscopic Poincaré return map as follows:

$$T_\lambda : \mathbf{R}^2 \to \mathbf{R}^2, \quad \mathbf{x}_0 \mapsto \mathbf{x}_1 \equiv T_\lambda(\mathbf{x}_0). \tag{A.2}$$

Let $\mathbf{u}$ be an l-periodic point of T_λ. Then, $\mathbf{u}$ satisfies the following equation:

$$T_\lambda^l(\mathbf{u}) - \mathbf{u} = 0, \tag{A.3}$$

where T_λ^l indicates T_λ applied l times. The characteristic equation is written as

$$\left| \frac{\mathrm{d}}{\mathrm{d}\mathbf{u}} T_\lambda^l(\mathbf{u}) - \mu \mathbf{I} \right| = 0, \tag{A.4}$$

where $\mathbf{I}$ is a two-dimensional identity matrix. The saddle-node, period-doubling, and Neimark–Sacker bifurcation parameters are obtained by substituting $\mu = 1$, -1, and $e^{i\theta}$ into Eq. (A.4), respectively, and solving Eqs. (A.3) and (A.4) simultaneously for $\mathbf{u}$ and λ. These simultaneous equations can be solved with Newton's method. The derivatives of the Poincaré return map T_λ with respect to $\mathbf{u}$ and λ can be derived from the following variational equations with respect to $\mathbf{u}$ and λ.

$$\begin{aligned}
\frac{\partial}{\partial \mathbf{u}} T_\lambda^l(\mathbf{u}) &= \frac{\partial}{\partial \mathbf{u}} \boldsymbol{\varphi}\left(\frac{2l\pi}{\omega}, \mathbf{u}, \lambda\right), \\
\frac{\partial}{\partial \lambda} T_\lambda^l(\mathbf{u}) &= \frac{\partial}{\partial \lambda} \boldsymbol{\varphi}\left(\frac{2l\pi}{\omega}, \mathbf{u}, \lambda\right), \\
\frac{\partial^2}{\partial \mathbf{u}^2} T_\lambda^l(\mathbf{u}) &= \frac{\partial}{\partial \mathbf{u}} \boldsymbol{\varphi}\left(\frac{2l\pi}{\omega}, \mathbf{u}, \lambda\right), \\
\frac{\partial^2}{\partial \mathbf{u} \partial \lambda} T_\lambda^l(\mathbf{u}) &= \frac{\partial^2}{\partial \mathbf{u} \partial \lambda} \boldsymbol{\varphi}\left(\frac{2l\pi}{\omega}, \mathbf{u}, \lambda\right),
\end{aligned} \tag{A.5}$$

where $\boldsymbol{\varphi}$ is a solution of Eq. (A.1) and satisfies $\boldsymbol{\varphi}(0, \mathbf{u}, \lambda) = \mathbf{u}$. The right-hand side of Eq. (A.6)

can be obtained from the first- and second-order variational equations as follows:

$$\frac{\mathrm{d}}{\mathrm{d}\tau}\frac{\partial\boldsymbol{\varphi}}{\partial\mathbf{u}} = \frac{\partial f}{\partial\mathbf{x}}\frac{\partial\boldsymbol{\varphi}}{\partial\mathbf{u}}, \quad \text{where } \left.\frac{\partial\boldsymbol{\varphi}}{\partial\mathbf{u}}\right|_{\tau=0} = \mathbf{I},$$

$$\frac{\mathrm{d}}{\mathrm{d}\tau}\frac{\partial\boldsymbol{\varphi}}{\partial\lambda} = \frac{\partial f}{\partial\mathbf{x}}\frac{\partial\boldsymbol{\varphi}}{\partial\lambda} + \frac{\partial f}{\partial\lambda}, \quad \text{where } \left.\frac{\partial\boldsymbol{\varphi}}{\partial\lambda}\right|_{\tau=0} = \mathbf{0},$$

$$\frac{\mathrm{d}}{\mathrm{d}\tau}\frac{\partial^2\boldsymbol{\varphi}}{\partial\mathbf{u}^2} = \frac{\partial f}{\partial\mathbf{x}}\frac{\partial^2\boldsymbol{\varphi}}{\partial\mathbf{u}^2} + \frac{\partial^2 f}{\partial\mathbf{x}^2}\left(\frac{\partial\boldsymbol{\varphi}}{\partial\mathbf{u}}\right)^2, \quad \text{where } \left.\frac{\partial^2\boldsymbol{\varphi}}{\partial\mathbf{u}^2}\right|_{\tau=0} = \mathbf{0},$$

$$\frac{\partial^2\boldsymbol{\varphi}}{\partial\mathbf{u}\partial\lambda} = \frac{\partial f}{\partial\mathbf{x}}\frac{\partial^2\boldsymbol{\varphi}}{\partial\mathbf{u}\partial\lambda} + \frac{\partial^2 f}{\partial\mathbf{x}^2}\frac{\partial\boldsymbol{\varphi}}{\partial\mathbf{u}}\frac{\partial\boldsymbol{\varphi}}{\partial\lambda} + \frac{\partial^2 f}{\partial\mathbf{x}\partial\lambda}\frac{\partial\boldsymbol{\varphi}}{\partial\mathbf{u}}, \quad \text{where } \left.\frac{\partial^2\boldsymbol{\varphi}}{\partial\mathbf{u}\partial\lambda}\right|_{\tau=0} = \mathbf{0}. \tag{A.6}$$

These variational equations represented by Eq. (A.6) are obtained by differentiating the following ODE with respect to $\mathbf{u}$ and λ as many times as necessary:

$$\frac{\mathrm{d}}{\mathrm{d}\tau}\boldsymbol{\varphi}(\tau,\mathbf{u},\lambda) = f(\boldsymbol{\varphi}(\tau,\mathbf{u},\lambda),\tau), \quad \text{where } \boldsymbol{\varphi}(0,\mathbf{u},\lambda) = \mathbf{u}. \tag{A.7}$$